Journal of Chromatography A, 1227 (2012) 82–95

Contents lists available at SciVerse ScienceDirect

Journal of Chromatography A

journal homepage: www.elsevier.com/locate/chroma

Measurement of the eddy dispersion term in chromatographic columns. II. Application to new prototypes of 2.3 and 3.2 mm I.D. monolithic silica columns

Fabrice Gritti, Georges Guiochon*

Department of Chemistry, University of Tennessee, Knoxville, TN 37996–1600, USA

ARTICLE INFO

Article history:
Received 2 November 2011
Received in revised form
14 December 2011
Accepted 19 December 2011
Available online 2 January 2012

Keywords:
Column technology
Mass transfer mechanism
HETP
Monolithic columns
Eddy diffusion
Trans-column effect

ABSTRACT

The mass transfer mechanisms in silica monolithic columns of the second generation were investigated, using four research samples (two 2.3 mm × 50 mm and two 3.2 mm × 50 mm silica rods) provided by their manufacturer. The heights equivalent to a theoretical plate (HETP) of these columns were measured in a range of mobile phase velocities, following a meticulous experimental protocol. The coefficients of the van Deemter equation (longitudinal diffusion term B/u_S, skeleton/eluent mass transfer resistance term Cu_S, and eddy diffusion term A) were determined. The protocol includes using the peak parking method (to determine the longitudinal diffusion term), an accurate model of effective diffusion in silica monolithic structures (to determine the skeleton/eluent mass transfer resistance term), and an accurate method to measure the column HETP and determine the eddy diffusion term. The results show that the minimum plate heights of these new monolithic columns ranges between 4 and 5 μm, three to four times lower than those observed for monolithic columns of the first generation. A detailed analysis of the eddy diffusion term demonstrates that this improvement in column efficiency is partly explained by the reduction of the domain size (the sum of the skeleton and throughpore sizes, −40%) but mostly by an increase of the radial homogeneity of the monolithic rods. The columns of this second generation exhibit residual trans-column relative velocity biases as low a 1.4% (instead of 3% for previous columns), a value which is comparable to those observed in 4.6 mm I.D. columns packed with sub-3 μm core–shell particles, with which they might become competitive.

1. Introduction

The preparation, production, and properties of continuous, bimodal porous silica monolithic materials began to be investigated in the late 1980s and during the 1990s [1–4]. Nakanishi was first to apply these materials to the preparation of a new type of columns for liquid chromatography [3]. The first silica monolithic columns were commercialized in 2000 (Chromolith, Merck, Darmstadt, Germany). While similar efforts were made during the same period to develop monolithic columns made of crosslinked polymers [5–7], the results were not as commercially successful.

Silica monolithic columns differ from particle-packed ones by the lack of a relationship between the volumes of the porous material (the porons) and of the spaces available to the mobile phase flow (the throughpores). The first commercial monolithic column had throughpore and poron sizes of 2.0 and 1.3 μm, respectively. At times when columns packed with 5 μm fully porous particles were dominating the field of column technology, these new columns seemed to bring hopes of great technical progress and commercial success. This was mainly supported by their large specific permeability (close to 8×10^{-14} m^2, several times larger than that of columns packed with 5 μm particles [8]), their fast solid/liquid mass transfer (due to the small size of the porons [9,10]), and their large sample capacity per unit adsorbent volume [11]. These columns provided a lower separation impedance than columns packed with 5 or 3.5 μm particles [12]. Nevertheless, a review of a decade of research and development work on monolithic columns [13] concluded that the advantage of these columns over conventional ones vanished during the 2000s. In spite of the considerable interest arisen in the scientific community by their novelty, these columns did not meet great commercial success, due to structural features inherent to their fabrication process, which cannot provide radially homogeneous 4.6 mm I.D. rods [14–16] nor long continuous rods, and to the consequences of their high external porosity.

A recent, rigorous investigation of mass transfer mechanisms in silica monolithic columns of this first generation confirmed that the main limitation to their applications in liquid chromatography was the excessively large contribution of the eddy diffusion term of their van Deemter equation [17]. For instance, at high linear superficial velocities (u_S > 5 mm/s), this term accounts for at least 95% of their total plate height, which is of the order of 20 μm [17].

* Corresponding author. Tel.: +1 865 974 0733; fax: +1 865 974 2667.
E-mail addresses: guiochon@utk.edu, guiochon@ion.chem.utk.edu (G. Guiochon).

0021-9673/$ – see front matter © 2011 Elsevier B.V. All rights reserved.
doi:10.1016/j.chroma.2011.12.065

Independent experiments based on the reconstruction of the morphology of silica monolithic structures confined in 100 μm glass capillary tubes [18–20] and on the calculated rate of the convective-diffusive mass transport process, concluded that the trans-throughpore and the short-range inter-throughpore eddy diffusion terms are not responsible for the low efficiency reported at high flow rates. Also, the trans-skeleton HETP term was found to be negligible in a wide range of analyte and skeleton properties [21]. In contrast, a visualization of the column defects (such as large voids or poor anchoring of the monolithic rod to the glass wall) showed dramatic effects on the column efficiency, meaning that inherent limitation to the performance of monolith rods is due to their trans-column structural heterogeneity and to the band dispersion caused by the inlet and outlet flow distributors. Nevertheless, for analysts for whom analysis time is not a constraint, silica monolithic columns prepared in long capillary tubes can provide very large resolution power [22–25]. Note, however, that the preparation methods and the structures of the silica monoliths in narrow capillary tubes and those in wider rods are considerably different.

Monolithic columns of the first generation found important applications as second columns in 2DLC [26] or also in preparative chromatography, albeit in an unusual format, a radial flow configuration [27]. Yet, the use of short monolithic columns of the first generation in fast LC remains hampered by their too large external porosity and domain size. No significant progress in their performance took place during the last decade. These columns are not competitive with modern columns [28], whether packed with modern sub-2 μm [29] or shell particles [30–34] when it comes to resolve highly complex mixtures. Recently, however, manufacturers began to release research samples which might be the harbinger of a second generation of monolithic columns. These prototype columns provide efficiencies approaching 200,000 plates per meter. Future trends in chromatography could well be to use highly permeable columns for fast separations requiring 10,000–35,000 theoretical plates. These new 5 cm long monolithic columns could be suitable for that purpose.

The goal of this work was to characterize and evaluate the kinetic performance of four distinct new prototype monolithic columns (two 2.3 mm × 50 mm and two 3.2 mm × 50 mm columns, Kyoto Monotech, Kyoto, Japan). The column length and their diameters were decided by the manufacturer. These columns are narrower than were those of the first generation of monolithic columns, which had an I.D. of 4.6 mm. A non-invasive protocol [35,36] already used to study the mass transfer mechanism in columns packed with core–shell particles [37–39] and the first generation of monolithic columns [17] was applied to these prototype columns. This method requires the measurement of (1) the true moments of the elution band profiles by numerical integration [40,41]; (2) the external porosity of the column packing by inverse size exclusion chromatography [42]; (3) the longitudinal diffusion coefficient of the van Deemter equation by the peak parking method [43–45]; and (4) the trans-skeleton mass transfer resistance term using the peak parking method and the best available model of effective diffusion in silica monolithic structures [46–48,36]. The sole contribution of the trans-rod velocity biases to the total eddy diffusion term is then estimated on the basis of the measurement of the trans-throughpore and short-range inter-throughpores eddy diffusion terms taken from the recent findings of Tallarek et al. [18] in the homogenous bulk region of capillary monolithic columns.

2. Theory

2.1. HETP equation for monolithic columns

The general HETP equation is the sum of three independent contributions [49], accounting, respectively, for (1) the longitudinal diffusion of the analyte during its migration along the column ($H_{Long.}$); (2) eddy diffusion due to all the sources of velocity biases taking place at different scales, from the inter skeleton to the rod diameter lengths, across and along the column (H_{Eddy}); and (3) the resistance to mass transfer by diffusion through the porous skeleton and between the eluent streamlets and the stagnant mesoporous volumes ($H_{Skel.}$). The usual HETP term associated with the so-called external film mass transfer resistance between the eluent stream and the surface of the skeleton was not considered in this work. This term has been investigated and used by chemical engineers for application to chemical reactors. It is related to the structure of the hydrodynamic layer through which the local velocity of the eluent continuously decreases from a maximum value in the center of the channels to zero at the surface of the solid skeletons. This term is already described by the trans-channel eddy diffusion term in the overall expression of H_{Eddy} [50]. The external mass transfer resistance at the surface of the stationary phase is actually negligible because the thickness of the stationary layer of eluent surrounding the skeleton is extremely small, with a thickness of the same order of magnitude as the surface roughness of the silica skeleton. Accordingly, the general HETP is written:

$$H = H_{Long.} + H_{Eddy} + H_{Skel.} \tag{1}$$

2.2. Determination of each individual HETP term

2.2.1. Longitudinal diffusion HETP term

The longitudinal diffusion term $H_{Long.}$ can be accurately and precisely measured by applying the peak parking method [51] (see Section 3.4). It is written [36]:

$$H_{Long.}(u_S) = \frac{B}{u_S} = 2\epsilon_e(1+k_1)\frac{D_{eff}}{u_S} = (1+k_1)\epsilon_e\frac{\Delta\sigma^2_{PP}}{\Delta t_p}\frac{u^2_{R,PP}}{u_S} \tag{2}$$

where B is the longitudinal diffusion coefficient, D_{eff} is the effective diffusion coefficient along the monolithic column, $\Delta\sigma^2_{PP}$ is the variance increment observed for an increment Δt_p of the peak parking time, $u_{R,PP}$ is the migration linear velocity of the analyte in the peak parking experiments, u_S is the superficial linear velocity of the eluent, k_1 is the zone retention factor, and ϵ_e is the external porosity of the monolithic column. By definition, k_1 is equal to:

$$k_1 = \frac{1-\epsilon_e}{\epsilon_e}\left[\epsilon_p + (1-\epsilon_p)K\right] \tag{3}$$

where K is the equilibrium constant of the analyte between the stationary phase and the bulk mobile phase and ϵ_p is the volume fraction of the solid adsorbent in the skeleton volume.

2.2.2. The liquid/skeleton resistance mass transfer term

The trans-skeleton mass transfer resistance term, $H_{Skel.}$, can be estimated provided that we know (1) the geometry or a configuration factor for the porous skeleton and (2) an accurate model of effective diffusion along a silica monolithic column providing an accurate estimate of the sample diffusivity through the porous skeleton, $D_{skel.}$. Based on scanning electron micrographs (SEM) of the monoliths, we can reasonably assume a simple cylindrical geometry for the structure of the interconnected silica porous skeletons [9]. The general expression of this HETP term is then written as [9]:

$$H_{Skel.} = \frac{1}{16}\frac{1}{1-\epsilon_e}\left(\frac{k_1}{1+k_1}\right)^2\frac{d^2_{skel.}}{D_{skel.}}u_S = C_{skel.}u_S \tag{4}$$

where $d_{skel.}$ is the diameter of the cylindrical skeleton, which was estimated based on the experimental values of the external porosity (see Section 3.7) and of the specific permeability (see Section 4.1) measured for the different columns used. We also applied a

direct rule of thumb using the reference average specific permeability of 7.9×10^{-14} m^2 for a standard silica monolith [8] with an external porosity of 0.70 [52] and an average throughpore size of $d_{throughpore}$ = 2 μm. Finally, we assume the permeability law of Ergun [53]:

$$d^2_{throughpore} = \frac{k_0 K_G (1-\epsilon_e)^2}{\epsilon_e^3} \quad (5)$$

where the constant K_G measured for the reference monolithic columns is equal to 193.

Finally, assuming that the porous skeletons are cylindrical, their diameter can be estimated to be:

$$d_{skel.} = d_{throughpore}\sqrt{\frac{1-\epsilon_e}{\epsilon_e}} \quad (6)$$

Regarding the diffusion coefficient $D_{skel.}$, a model of effective diffusion in a monolithic column must be selected. In this work, we will test successively four models in binary composite media (bulk eluent and solid porous skeleton volumes):

- 1 *The time average model*
  This model has been abundantly used in liquid chromatography for its simplicity. It is based on the additivity of the mass fluxes in each phase. The effective diffusion coefficient, D_{eff}, is then written [36]:

$$D_{eff} = \frac{\gamma_e + ((1-\epsilon_e)/\epsilon_e)\Omega}{1+k_1} D_m \quad (7)$$

  where Ω is the ratio of the sample diffusivity in the porous adsorbent, $D_{skel.}$, and the bulk diffusion coefficient, D_m. It is lower than unity for non-retained species because diffusion is restricted to the mesoporous volume and above unity for retained compounds in RPLC, due to the additional contribution of surface diffusion to the total sample diffusivity [54,55,46]. γ_e is the external obstruction factor and can be expressed as a function of the external porosity for a monolithic column by [56,36]:

$$\gamma_e = \frac{1-\xi_2}{2-\epsilon_e(1+\xi_2)} \quad (8)$$

  This equation was derived from the general stochastic theory of effective diffusion, which was developed by Torquato and assumes randomly distributed and non-porous cylinders. For instance, for ϵ_e = 0.7, γ_e is equal to 0.73, a value which coincides with the one obtained by morphology reconstruction and mass transport calculations in silica monolithic structures when the parameter ξ_2 is adjusted to 0.11 [18].
- 2 *The Landauer model*
  This more sophisticated model considers the solid skeleton as a set of microscopic inhomogeneities dispersed randomly in the bulk mobile phase. The solution for D_{eff} is given by [57,58,55]:

$$D_{eff} = \frac{a + \sqrt{a^2 + (1/2)\Omega}}{\epsilon_e(1+k_1)} D_m \quad (9)$$

  with

$$a = \frac{1}{4}[3\epsilon_e - 1 + \Omega(2-3\epsilon_e)] \quad (10)$$

- 3 *The Garnett model*
  This approximate model assumes that the external eluent forms a cylindrical concentric shell around the elements of the porous skeleton, the diffusion direction being perpendicular to the axis of these cylinders. It assumes furthermore that any interstitial space is filled with smaller and smaller inclusions, down to the infinitesimally small ones. The effective diffusion coefficient is written [59,48,47]:

$$D_{eff} = \frac{1}{\epsilon_e(1+k_1)} \frac{1+\Omega-(1-\epsilon_e)(1-\Omega)}{1+\Omega+(1-\epsilon_e)(1-\Omega)} D_m \quad (11)$$

- 4 *The Torquato model*
  This model is based on a probabilistic theory [56]. For a random dispersion of the skeleton cylinders, it is written [60,61]:

$$D_{eff} = \frac{1}{\epsilon_e(1+k_1)} \left[\frac{1+(1-\epsilon_e)\beta - \epsilon_e\xi_2\beta^2}{1-(1-\epsilon_e)\beta - \epsilon_e\xi_2\beta^2}\right] D_m \quad (12)$$

  with

$$\beta = \frac{\Omega - 1}{\Omega + 1} \quad (13)$$

  and with ξ_2 = 0.11 in silica monolithic structures [36].

These four models will be tested by comparing the expected values of Ω for a non-retained compound (uracil) and the experimental results. The expression of Ω is given by [62]:

$$\Omega = \epsilon_p \gamma_p F(\lambda_m) \quad (14)$$

where the product $\gamma_p F(\lambda_m)$ is the restricted diffusion coefficient due to the channel tortuosity, channel constriction, and the hindrance diffusion in confined geometry. This product is a function of the particle porosity, ϵ_p, and of the average pore size, $\overline{d_{pore}}$. The reference experimental values are available in the literature for particle porosities ϵ_p = 0.61, 0.67, 0.69, 0.68 and 0.69 and average pore sizes d_{pore} = 60, 108, 120, 160, and 180 Å, respectively [63]. They increase from 0.37, 0.52, 0.54, 0.66 to 0.70. The adjustment of the actual restricted diffusion coefficient to the measured particle porosities and average pore sizes can be estimated for open cylindrical pores by [64]:

$$\gamma_p = 1 - \frac{2}{3}(1+\epsilon_p)(1-\epsilon_p)^{3/2} \quad (15)$$

and [65]

$$F(\lambda_m) = (1-\lambda_m)^2(1 - 2.1044\lambda_m + 2.089\lambda_m^3 - 0.948\lambda_m^5) \quad (16)$$

with

$$\lambda_m = \frac{d_{analyte}}{\overline{d_{pore}}} \quad (17)$$

where $d_{analyte}$ is the analyte size.

The average pore size is measured from the intersection between the exclusion and the intrusion branches of the ISEC plots (see Table 1). The molecular size of uracil is $d_{analyte}$ = 5.0 Å. The experimental values expected for Ω are listed in Table 1. The selected model of effective diffusion will be the one that predicts Ω values closest to these semi-empirical values.

2.2.3. The total eddy diffusion term

The eddy diffusion term is obtained simply by subtracting the longitudinal diffusion and the liquid/skeleton mass transfer resistance terms from the measured value of the overall HETP

$$H_{Eddy} = H - H_{Long.} - H_{Skel.} \quad (18)$$

The eddy diffusion term itself is the sum of three main contributions including the impact of the trans-throughpore ($H_{Throughpore}$), the short-range inter-throughpore (H_{Short}), and the trans-rod velocity biases ($H_{Trans\text{-}rod}$) [17,18]:

$$H_{Eddy} = H_{Throughpore} + H_{Short} + H_{Trans\text{-}rod} \quad (19)$$

The HETP terms $H_{trans\text{-}throughpore}$ and $H_{inter\text{-}throughpore}$ could be determined if the radial structure of the silica monolith is perfectly homogeneous. This was done by morphology reconstruction,

Table 1
Physico-chemical property of the four silica-C_{18} monolithic columns prepared by Kyoto Monotech measured in our lab.

Column's serial number	Column's dimension I.D. [mm] × length [mm]	Total porosity[a] (ϵ_t)	External porosity[b] (ϵ_e)	Shell porosity[c] (ϵ_p)	Average mesopore diameter[d] [Å] (d_{pore})	Expected shell diffusivity[h] (Ω)	Average skeleton diameter[e] [μm] ($d_{skel.}$)	Average throughpore diameter[f] [μm] ($d_{throupore}$)	Permeability[g] [cm^2] (k_0)
N648	3.2 × 50	0.745	0.613	0.341	65	0.09	1.03	1.30	1.35×10^{-10}
N655	3.2 × 50	0.847	0.692	0.519	199	0.34	0.64	0.95	1.65×10^{-10}
N731	2.3 × 50	0.847	0.664	0.545	152	0.34	0.85	1.19	1.90×10^{-10}
N733	2.3 × 50	0.877	0.696	0.595	145	0.40	0.69	1.04	2.06×10^{-10}

[a] Value obtained from the corrected elution volume of ethylbenzene in pure tetrahydrofuran.
[b] Value obtained from the extrapolation of the exclusion branch of the ISEC plots.
[c] Value calculated from $(\epsilon_t - \epsilon_e)/(1 - \epsilon_e)$.
[d] Value obtained from the intersection of the exclusion and intrusion branches of the ISEC plots.
[e] Value estimated assuming cylindrical pore and skeleton shapes.
[f] Value obtained from the Ergun permeability law and the reference permeability of commercial Chromolith column ($k_0 = 7.9 \times 10^{-10}$ cm^2 and $d_{throughpore} = 2.0$ mm).
[g] Value obtained from the corrected pressure drop measurements ($T = 297.7$ K, eluent: CH_3CN/H_2O, 55/45, v/v).
[h] Value expected for a non-retained compound (uracil) from the present ISEC data, Mitzithras data [63], Pismen [64], and Renkin [65] correlations.

using confocal laser scanning microscopy (CLSM), and by calculating the mass transport properties in the center zone of commercial 100 μm × 600 mm monolithic columns with a nominal macropore size of 2 μm and a nominal skeleton thickness of 1 μm [18]. These terms are written:

$$H_{Throughpore} = 0.133 \frac{u_S d_{skel.}^2}{D_m} \tag{20}$$

and

$$H_{Short} = 1.641 \frac{u_S d_{skel.}^2}{D_m} \frac{1}{1 + 1.154(u_S d_{skel.}/D_m)} \tag{21}$$

The trans-column eddy diffusion term, $H_{Trans\text{-}rod}$, results from a complex combination of the radial velocity distribution, the average radial dispersion coefficient, and the band broadening contributions of the inlet and outlet distributors, which distribute the in-going stream across the inlet cross-section of the column and collect the out-going streamlets. This term is unknown but can be estimated by subtracting the first two terms from the overall eddy diffusion term or:

$$H_{Trans\text{-}rod} = H_{Eddy} - H_{Throughpore} - H_{Short} \tag{22}$$

2.3. Determination of the true chromatographic HETP

The first and second central moments of all the peak profiles eluted from the extra-column volume (instrument alone, using a ZDV union connector) and from the whole system (instrument + column) were measured sequentially by numerical integration of the full concentration profiles, using a home-made program recently published [41]. Prior to the moment measurement, each elution profile was treated according to the following procedure illustrated in Fig. 1. The time of calculation required is less than one minute. In part I of this series of papers, which dealt with columns of the first generation of monolithic columns [17], the same measurements were performed manually, one peak after the other. The new program considerably accelerates the processing of experimental results. Both methods provide exactly the same results, within less than 0.1% (first moment) and 0.5% (second moment) but the time required for each moment measurement is reduced from about two hours to a minute.

First, a linear baseline correction of the whole chromatogram is performed to correct for the baseline drift of the signal that is assumed to be linear during the whole run. Second, the width of the integration interval is defined as a multiple, n, of the peak-width at half-height ($n = 4$ for the uracil and the naphthalene peaks). Thirdly, the peak apex is positioned at a precise fraction, p, of the width of the integration interval ($p = 0.45$ for the uracil and the naphthalene peaks), to account for peak tailing. Fig. 1A and B shows typical peak profiles of uracil and naphthalene, respectively, recorded on the 2.3 mm × 50 mm N733 column, with baseline correction (solid green line), the boundaries and the position of the integration interval (delimited by the left and right red vertical segments) of the peak profile (solid blue curve), and their best fit to a Gaussian peak function (solid purple curve). The flow rate was set at 2.0 mL/min. The discrepancies between the Gaussian curve and the experimental peak profile justify the use of this numerical method for the determination of the true HETPs of all four monolithic columns studied in this work.

Finally, the first and the second central moments of the concentration profiles, μ_1 and μ_2', were calculated using the recorded data points, following these equations [40]:

$$\mu_1 = \frac{\sum_{i=1}^{i=N-1}(C_i + C_{i+1})(t_i + t_{i+1})}{2\sum_{i=1}^{i=N-1} C_i + C_{i+1}} \tag{23}$$

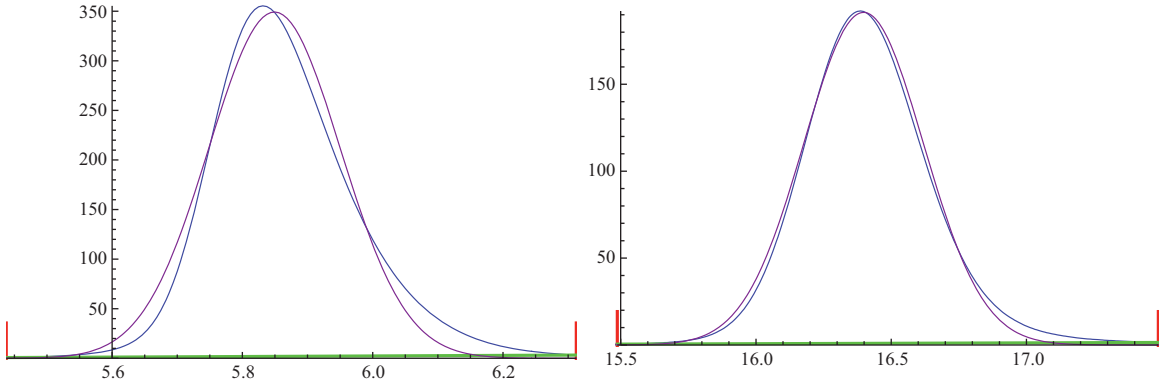

Fig. 1. Accurate measurements of the first and second central moments of uracil (left) and naphthalene (right) eluted from a 2.3 mm × 50 mm silica monolithic column at a flow rate of 2.0 mL/min. T = 297.1 K. The units are absorbance in mAU for the y-axis and time in second for the x-axis. See detailed explanation in the text in Section 2.3. (For interpretation of the references to color in the text, the reader is referred to the web version of the article.)

$$\mu'_2 = \frac{\sum_{i=1}^{i=N-1}(C_i + C_{i+1})((t_i + t_{i+1})/2 - \mu_1)^2}{\sum_{i=1}^{i=N-1} C_i + C_{i+1}} \quad (24)$$

the values of the first and second central moments are accurate within 0.1 and 2%, respectively.

The corrected HETP, H, is then given by:

$$H = L\frac{\mu'_2 - \mu'_{2,ex}}{(\mu_1 - \mu_{1,ex})^2} \quad (25)$$

where L is the column length and $\mu_{1,ex}$ and $\mu'_{2,ex}$ are the first and the second central moments of the corresponding extra-column band profiles.

The precision of the column plate height is given by

$$\left|\frac{\Delta H}{H}\right| = \left|\frac{\Delta\mu'_2}{\mu'_2}\right|\left(\frac{\mu'_2 + \mu'_{2,ex}}{\mu'_2 - \mu'_{2,ex}}\right) + 2\left|\frac{\Delta\mu_1}{\mu_1}\right|\left(\frac{\mu_1 + \mu_{1,ex}}{\mu_1 - \mu_{1,ex}}\right) \quad (26)$$

the accuracy of the HETP values are then between 2% and 12%, depending on the retention factor and the column size.

The relative random errors (for duplicate injections made at each flow rate) on the first moments are smaller than 0.1% (uracil) and 0.05% (naphthalene). The relative random errors made on the second central moments are smaller than 1.0% (uracil) and 0.8% (naphthalene), once the right and left cuts are fixed as above mentioned. The remarkable repeatability of the injection system of the 1290 Infinity system permits the achievement of this excellent precision of H measurements. Therefore, this integration approach provides both accurate and precise HETP data that analysts can trust for a further detailed analysis of the mass transfer mechanism [40]. Accordingly, if the extra-column contributions were negligible, as they are for strongly retained compounds eluted from wide columns, the largest random error would be less than 1.2%. With small I.D., efficient columns and non-retained compounds, the variance contribution of the system to overall band broadening becomes large. For instance, with the 2.3 mm I.D. monolithic columns studied in this work, this system contribution can account for more than 70% of the total peak variance and the largest random error is about 6.5%. For the 3.2 mm I.D. column, this error drops to only 3.3%.

3. Experimental

3.1. Chemicals

The mobile phase was a mixture of acetonitrile and water (55/45, v/v). Tetrahydrofuran was used as the eluent for the inverse size-exclusion chromatography (ISEC) measurements. All these solvents were HPLC grade from Fisher Scientific (Fair Lawn, NJ, USA). The mobile phases were filtered before use on a surfactant-free cellulose acetate filter membrane, 0.2 μm pore size (Suwannee, GA, USA). Eleven polystyrene standards (MW = 590, 1100, 3680, 6400, 13,200, 31,600, 90,000, 171,000, 560,900, 900,000, and 1,877,000) were used to acquire ISEC data. They were purchased from Phenomenex (Torrance, CA, USA). The low molecular weight compounds used in this work were uracil and naphthalene, with a minimum purity of 99% (Fisher Scientific).

3.2. Apparatus

The 1290 Infinity HPLC system (Agilent Technologies, Waldbroen, Germany) liquid chromatograph used in this work includes a 1290 Infinity Binary Pump with Solvent Selection Valves and a programmable auto-sampler. The injection volume was set at 0.5 μL (for 2.3 mm I.D. columns) and 1 μL (for 3.2 mm I.D. columns) and was drawn into one end of the 20 μL injection loop. The instrument is equipped with a two-compartment oven and a multi-diode array UV-VIS detection system. The system is controlled by the Chemstation software. The sample trajectory in the equipment involves the successive passage of its band through

- A 20 μL injection loop attached to the injection needle. The design of the injection system is such that the volume of sample drawn into the loop is the volume of sample injected into the column.
- A small volume needle seat capillary (115 μm I.D., 100 mm long), ≃1.0 μL, located between the injection needle and the injection valve. The total volume of the grooves and connection ports in the valve is around 1.2 μL.
- One of the different types of capillary tubes which were placed before and after the column, a 65 μm I.D. (brown tubings), a 115 μm I.D. (red tubings), a 140 μm I.D. (green tubings), all 40 cm long, and a 130 μm 56 cm long Viper capillary tube offered by the manufacturer (Dionex, Germering, Germany) were used. Their total volumes are 1.3, 4.2, 6.2, and 7.4 μL, respectively.
- A small volume detector cell, 0.8 μL, 10 mm path.

The extrapolation to a zero flow rate of the extra-column volume using the Viper capillary tube measured for 1.0 μL injections of uracil and naphthalene tracers in the flow rate range between 0.05 and 2.0 mL/min provides an average extra-column volume of 11.4 μL. According to the dimensions just cited, we should expect a volume of 0.5 (injection volume) + 1.0 (needle seat capillary) + 1.2 (injection valve) + 7.4 (inlet and outlet capillaries) + 0.4 (detector cell) = 10.5 μL. Given the wide range of the specifications (±20%) for the inner diameter of the connecting capillary tubes, these two

values are in good agreement. We measured an offset time of about 0.04 s between the moments when the zero time is recorded and when the sample leaves the injection needle. Note that the extra-column peak variance measured with the Viper connector rapidly increases from 2.9 μL^2 at 0.05 mL/min to 11.5 μL^2 at 0.6 mL/min and remains nearly constant at higher flow rates.

3.3. Columns

Four research monolith samples were generously offered to us by Kyoto Monotech (Kyoto, Japan). The two 2.3 mm × 50 mm columns, N731 and N733, are from the same batch of silica gel. The 3.2 mm × 50 mm columns, N648 and N655, were made from feeds having different compositions. Their physico-chemical characteristics (total, external and internal porosities, average mesopore size, predicted ratio of poron to bulk diffusivities for a non-retained compound, average skeleton diameter, average throughpore diameter, and specific permeability) were derived in this work. They are listed in Table 1. The modified silica-C_{18} surface was fully endcapped according to a proprietary process. The 4.6 mm × 100 mm column packed with 1.9 μm non-porous silica particles that we used for the measurement of the diffusion coefficient of uracil and naphthalene was a generous gift from Phenomenex (Torrance, CA, USA).

Note that the columns N731 and N733 are slightly larger than 2.3 mm. The measurement of the diameter of the mold in which the silica gel was prepared provides a diameter of 2.33 mm. The column diameter depends also on the extend of shrinkage of the rod during its preparation.

The prototype monolithic columns used in this work contain two frits (one at the inlet, the other at the column outlet) with a porosity of 0.5. Their dimensions are 2 mm × 1 mm and 3 mm × 1 mm, e.g. total volumes of 3.1 μL and 7.1 μL in the 2.3 and 3.2 mm I.D. columns, respectively. These frits are truncated cones (total volume, 1.6 μL). Considering that the total porosity of the 5 cm long monolithic columns is 0.85, these volumes account for about $4.7/(0.85 \times \pi \times 0.115^2 \times 5) = 2.7\%$ and $8.7/(0.85 \times \pi \times 0.15^2 \times 5) = 2.9\%$ of the total hold-up volume of the 2.3 and 3.2 mm I.D. columns, respectively, which is a significant fraction of the extra-column volume. *Stricto sensu*, these contributions to the extra-silica monolithic rod volume are 11.4 + 4.7 = 16.1 μL (2.3 mm I.D.) and 11.4 + 8.7 = 20.1 μL (3.0 mm I.D.), respectively. Therefore, the contribution to band broadening that take place during migration of the band along the frits and the truncated cones cannot be neglected compared to the band broadening taking place in the 1290 HPLC system volume. Because, the variance contribution caused by the passage of the band through the frits and the truncated cones is unknown, it will be considered as part of the contribution of the monolithic column.

3.4. Peak parking (PP) measurements

The PP method was used to measure the longitudinal diffusion HETP terms ($H_{Long.}(u_S)$) of the monolithic columns studied and the effective diffusivities ($D_{skel.}$) of the samples through their porous skeleton. This technique was pioneered by Knox in gas [66] and liquid chromatography [43] and was recently used to measure the internal obstruction factor of porous silica-C_{18} particles [44] and the bulk diffusion coefficients of sample molecules in the liquid mobile phase [67,68].

In the PP experiments reported, 1 μL (for 2.3 mm I.D. columns) or 2 μL (for 3.2 mm I.D. columns) of a dilute sample solution (<0.5 g/L) was injected at a low, constant flow rate (0.100 and 0.194 mL/min for the 2.3 and 3.2 mm I.D. columns, respectively, in order to keep the same low superficial linear velocity, e.g. a similar low pressure drop along the column during the elution). The column was eluted during the time necessary for the non-retained sample (uracil) to reach about 3/4 of the length of the column. Since the retention factors measured for naphthalene on the N731, N733, N648, and N655 monolithic columns were 2.0, 1.9, 3.4, and 1.3, respectively, this compound was parked at about 1/4, 1/4, 1/5, and 1/3 of the lengths of these columns. When the uracil band has reached the desired position, the flow is abruptly stopped and the sample is left free to diffuse around the position that it reached along the column, during a certain time (the parking time, t_p). This parking time was successively set at 1, 15, 30, 60, and 120 min. All the results of the peak variance measured as a function of the parking time are gathered in Fig. 2. They will be discussed later.

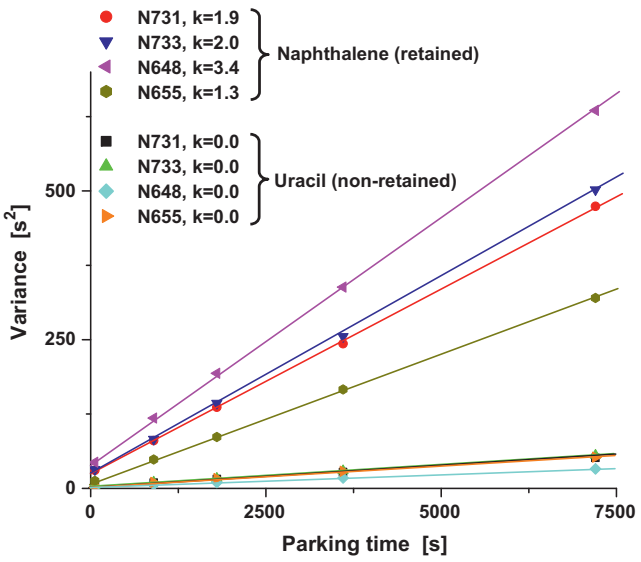

Fig. 2. Plots of the variances of the eluted band profiles recorded during the peak parking experiments *versus* the peak parking time. Four different monolithic columns (N731, N733, N648, N655) and two solutes (uracil and naphthalene) were used. For all columns the superficial linear velocity was fixed at 0.040 cm/s. The peak parking times were set at 1, 15, 30, 60, and 120 min.

The slope of the plot of the elution peak variance *versus* the peak parking time, $\Delta\sigma^2_{PP}/\Delta t_p$, provides a direct measure of the effective diffusion coefficient along the packed bed (D_{eff}) and an estimate of the sample diffusivity through the porous skeleton ($D_{skel.} = \Omega D_m$), as explained in Sections 2.2.1 and 2.2.2, respectively.

3.5. Measurement of the bulk diffusion coefficients D_m

The diffusion coefficients of uracil and naphthalene were measured by applying the peak parking method, using a 100 mm × 4.6 mm column packed with solid, non-porous silica particles (1.9 μm). The external obstruction factor, γ_e, of this column was obtained from the effective diffusion coefficient ($D_{eff} = \gamma_e D_m$) of thiourea in pure water at $T = 298.15$ K ($D_m = 1.33 \times 10^{-5}$ cm²/s [69,70]). Accordingly, we measured $\gamma_e = 0.65$ [17]. The same measurement was repeated with uracil and naphthalene in a mixture of acetonitrile and water (55/45, v/v), to evaluate the kinetic performance of the monolithic columns studied in this work. The flow rate was fixed at 0.4 mL/min. UV detection was done at a wavelength of 274 nm with a bandwidth of 4 nm. The peak parking times were set at 1, 60, 120, 180, and 240 min. The temperature profile T_{PP} was recorded during the whole PP experiments. Due to slight temperature variations overnight (±1 K during the 10 h sequence run), T_{PP} was taken as the mean of the five average temperatures recorded during each parking period. The viscosity of the eluent at the temperature T_{PP} was taken from the literature [71].

Table 2
Temperatures (T), diffusion coefficients (D_m), zone retention factor (k_1), effective diffusion coefficients (D_{eff}), ratio of the shell diffusivity to the bulk diffusion (Ω), reduced longitudinal diffusion coefficients (B), and solid–liquid mass transfer coefficient (C_p) measured for the non retained compound uracil.

Column's serial number	Column's dimension I.D. [mm] × length [mm]	T [K]	D_m [cm^2/s]	k_1	D_{eff} [cm^2/s]	Ω	B [cm^2/s]	$C_{skel.}$ [μs]
N648	3.2 × 50	297.4	1.06×10^{-5}	0.17	6.70×10^{-6}	0.09	0.96×10^{-5}	8.2
N655	3.2 × 50	297.6	1.06×10^{-5}	0.23	7.77×10^{-6}	0.38	1.30×10^{-5}	36.6
N731	2.3 × 50	297.3	1.06×10^{-5}	0.25	7.73×10^{-6}	0.42	1.28×10^{-5}	12.1
N733	2.3 × 50	297.3	1.06×10^{-5}	0.24	7.73×10^{-6}	0.42	1.34×10^{-5}	8.4

Table 3
Same as in Table 2, except the compound, naphthalene.

Column's serial number	Column's dimension I.D. [mm] × length [mm]	T [K]	D_m [cm^2/s]	k_1	D_{eff} [cm^2/s]	Ω	B [cm^2/s]	$C_{skel.}$ [μs]
N648	3.2 × 50	297.4	1.27×10^{-5}	4.39	6.70×10^{-6}	3.00	4.03×10^{-5}	29.8
N655	3.2 × 50	297.6	1.27×10^{-5}	1.89	7.77×10^{-6}	2.91	3.54×10^{-5}	10.8
N731	2.3 × 50	297.3	1.27×10^{-5}	2.78	7.73×10^{-6}	3.51	4.17×10^{-5}	16.2
N733	2.3 × 50	297.3	1.27×10^{-5}	2.71	7.73×10^{-6}	3.70	4.12×10^{-5}	11.1

The diffusion coefficient $D_m(T)$ at temperature T is obtained from the peak parking data measured at temperature T_{PP} by [51]:

$$D_m(T) = \frac{1}{2\gamma_e} \frac{\Delta\sigma^2_{PP}(T_{PP})}{\Delta t_p} \frac{L^2}{t_R^2} \frac{T}{T_{PP}} \frac{\eta(T_{PP})}{\eta(T)} \quad (27)$$

where L is the column length, t_R is the retention time of the compound with no flow interruption, and $\eta(T)$ and $\eta(T_{PP})$ = 0.847 cP are the eluent viscosities at temperatures T and T_{PP} = 293.6 K.

All the bulk molecular diffusion coefficients are given in the fourth column of Table 2 (uracil) and Table 3 (naphthalene) for the temperatures T (third column) recorded during the measurement of the column HETP as described below.

3.6. HETP plots

For all columns, the same sequence of superficial linear velocities (from 0.20 to 5.62 mm/s) was applied. The corresponding flow rates were set at 0.05, 0.10, 0.20, 0.30, 0.40, 0.50, 0.60, 0.70, 0.80, 1.00, 1.20, and 1.40 mL/min for the 2.3 mm I.D. columns and 0.097, 0.194, 0.387, 0.581, 0.774, 0.968, 1.161, 1.355, 1.549, 1.936, 2.323, and 2.710 mL/min for the 3.2 mm I.D. columns. The sampling rate was adjusted to 2.5, 5, 10, 20, 20, 40, 40, 40, 40, 80, 80, 80, 80, 160, and 160 Hz, respectively, in order to record peak profiles with a comparable number of data points (>75) at all flow rates. 0.50 and 0.97 μL of the sample solution (concentration <0.5 g/L) was injected into the 2.3 and 3.2 mm I.D. columns, respectively, and the chromatograms were recorded at the same wavelength of 265 nm. For all samples, a constant bandwidth of 4 nm was selected. The temperature was set by the laboratory air-conditioner at 297.4 ±0.5 K.

3.7. ISEC experiments

The ISEC experiments were carried out with neat THF as the eluent. Twelve polystyrene standards were used with molecular weight between 100 and 2 millions Dalton. This covers a wide range of molecular sizes between 4 and 950 Å. The flow rate was set at 0.12 and 0.24 mL/min for the 2.3 mm × 50 mm and 3.2 mm × 50 mm monolithic columns, respectively. The external porosity was determined from the extrapolated elution volumes of the exclusion branches to a molecular radius of zero divided by the column tube volume (0.208 and 0.402 cm^3). The results are listed in Table 1.

4. Results and discussion

In the first part of this work, we report and discuss the permeability of the four monolithic columns provided by the manufacturer (Kyoto Monotech) and estimate the average throughpore size, the average skeleton size, and the average mesopore size from the ISEC plots. As a reference, note that the first generation of monolithic columns commercialized by Merck in 2000 had an average specific permeability of 7.9×10^{-14} m^2 [8,4,13], an average throughpore size of 2 μm [12,4], an average skeleton size of 1.3 μm [12,4], and an average mesopore size of 120 Å before C_{18} derivatization [4]. In a second part, we accurately measured the overall kinetic performance of these new monolithic columns for a non-retained and a retained compounds, using a general experimental protocol, designed recently [51,36]. Finally, we estimate the residual trans-column heterogeneity of these columns from their trans-rod eddy diffusion term and we compare it to that of the first generation of monolithic columns.

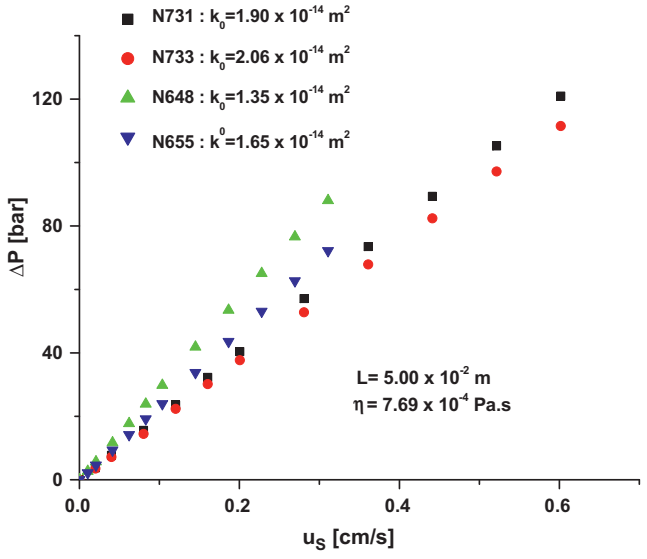

Fig. 3. Column pressure drops recorded as a function of the superficial linear velocity.

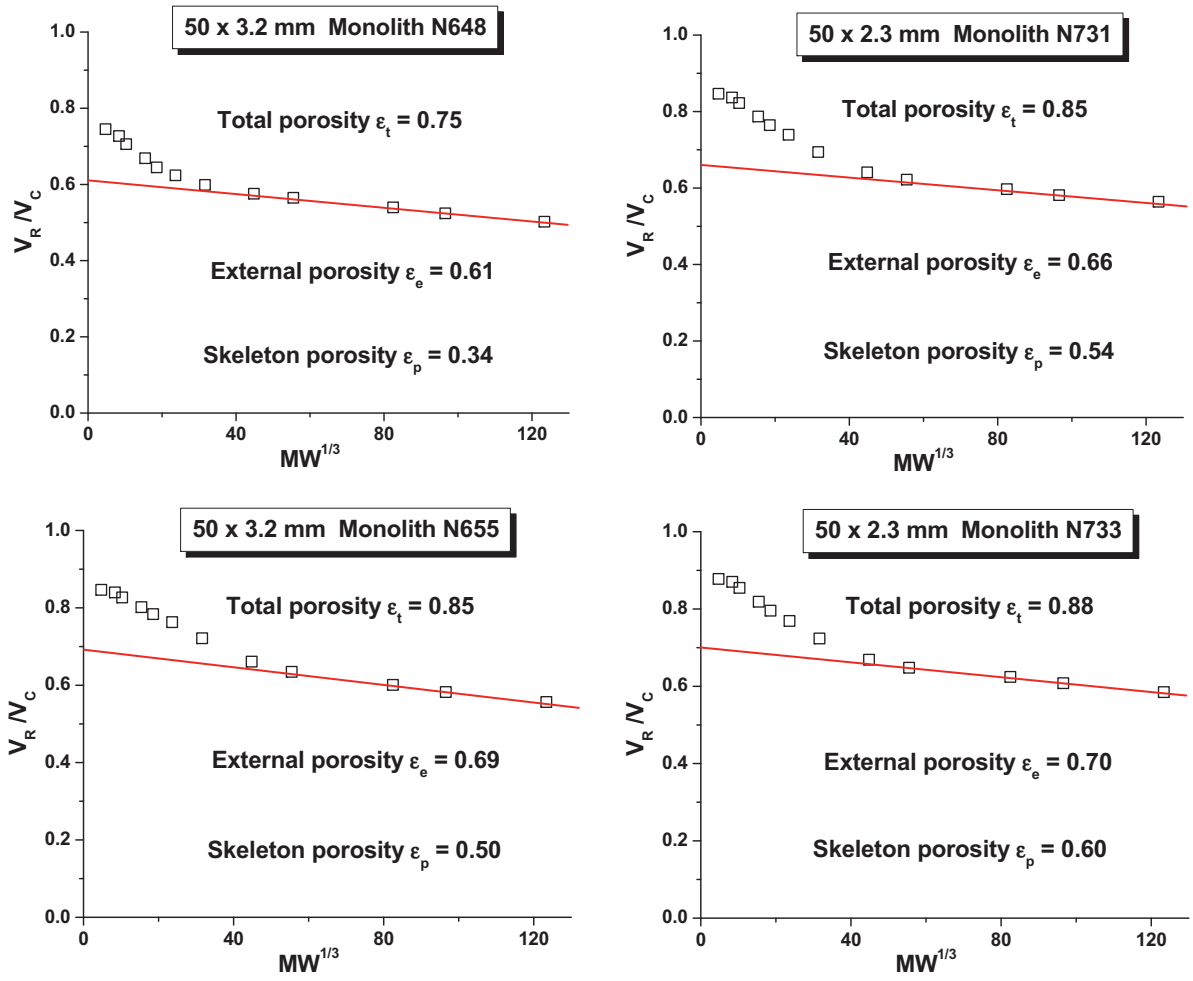

Fig. 4. ISEC plots constructed from the elution volumes of twelve polystyrene standards normalized to the column tube volume. The *y*-axis represents the ratio of the elution volume, V_R, of the polystyrene standards to the volume of the empty column tube, V_C. MW is the molecular weight.

4.1. Permeability of the monolithic columns

The pressure drops along the monolithic columns were measured by subtracting the system pressure drop (measured in the absence of column) from the total pressure drop (measured in the presence of the column) at flow rates of 0.05, 0.10, 0.20, 0.30, 0.40, 0.50, 0.70, 0.90, 1.10, 1.30, and 1.50 mL/min. The eluent was a mixture of acetonitrile and water (55/45, v/v) and the temperature was recorded at 297.7 K. The viscosity of the mobile phase is then $\eta = 0.767$ cP. The plots of these corrected pressure drops *versus* the applied flow rate are shown in Fig. 3 for the four columns studied in this work. The pressure drop, ΔP, is given by the general permeability equation [49]:

$$\Delta P = \frac{\eta L}{\pi R_c^2 k_0} F_v \tag{28}$$

For all the columns, the slopes of the linear plots shown in Fig. 3 were measured for $u_S < 0.1$ cm/s. These slopes provide the estimate of the specific permeability, k_0, of each column, knowing the internal radius of the columns ($R_c = 0.115$ and 0.160 cm). The values are 1.90, 2.06, 1.35, and 1.65×10^{-14} m^2 for the columns N731, N733, N648, and N655, respectively. They are four to six times smaller than those obtained for the first generation of monolithic columns (7.9×10^{-14} m^2). This shows that the domain size is significantly smaller. The external porosities of columns N731, N733, N648, and N655 were derived from the ISEC plots shown in Fig. 4A–D. They were found to be 0.66, 0.70, 0.61, and 0.69, respectively. Eq. (5) with $K_G = 193$ was used in order to estimate the average throughpore size of these new columns. This value of $K_G = 193$ was derived from the specific permeability of the reference silica monolithic material with $d_{throughpore} = 2.0$ μm, $\epsilon_e = 0.70$, and $k_0 = 7.9 \times 10^{-14}$ m^2. Accordingly, the average throughpore sizes of columns N731, N733, N648, and N655 are equal to 1.19, 1.04, 1.30, and 0.95 μm, respectively. On the average, the throughpore size decreased from 2.0 to 1.1 μm, a 45% relative decrease Eq. (6) was used to estimate the average skeleton sizes, giving values of 0.85, 0.69, 1.03, and 0.64 μm, respectively. Thus, the average skeleton size has decreased from 1.3 to 0.8 μm, a relative reduction of 38%. Overall, the domain size (sum of the throughpore and the skeleton sizes) has decreased from 3.3 to 1.9 μm, a 42% relative diminution.

The intersection of the exclusion branch with the intrusion branch provides a good estimate of the average mesopore size after bonding of the silica surface with C_{18} chains. Values of 152, 145, 65, and 199 ± 10 Å were found. All these data are listed in Table 1, for later use to estimate the intra-skeleton diffusivity of a non-retained compound (uracil) and select the best model of effective diffusion in monolithic columns.

4.2. Extra-column tubings

Before measuring the HETP plots of the four monolithic columns corrected for the extra-column contributions, we selected the connecting tubes that provide the best compromise between two antagonist properties: the extra-column pressure drop

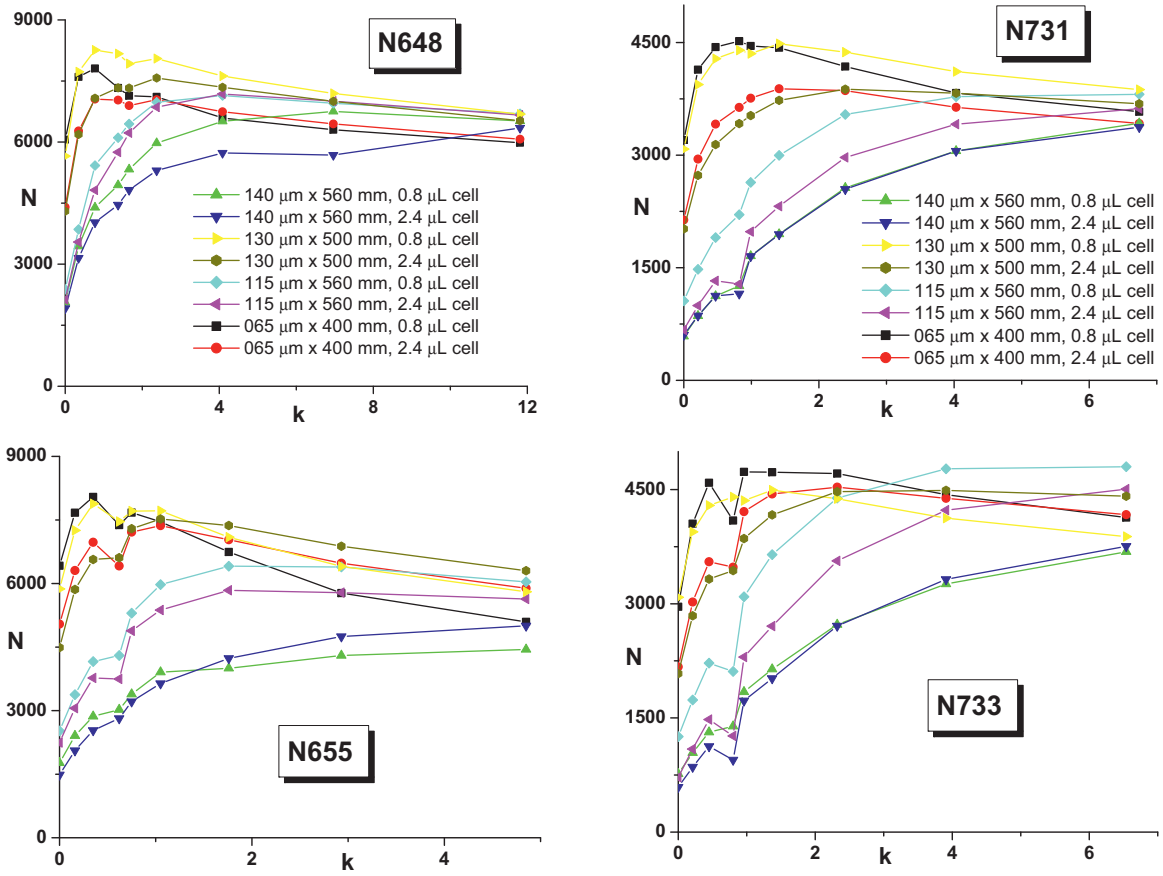

Fig. 5. Efficiencies of the four monolithic columns measured for eight different system configurations as a function of the retention factor of nine analytes. See text for more details.

contribution and the extra-column band broadening contribution. Both should be kept as small as possible. Four connecting tube geometries were used: 65 μm × 400 mm (Polymer tubings), 115 μm × 400 mm (metallic tubings), 140 μm × 400 mm (metallic tubings), and 130 μm × 500 mm (Viper tubings). The endfittings of the metal tubes are irreversibly fixed to both ends of these tubes. In addition, two detector cells of volumes 0.8 and 2.4 μL were tested with each connecting tube. The mobile phase flow rate was set at the relatively large values of 1.6 (for N731 and N733) and 2.0 mL/min (for N648 and N655), in order to maximize the contributions of the extra-column fittings and to operate the columns at the maximum inlet pressure that they may tolerate (≃200 bar). The average total pressure drop recorded for these four columns were 277, 168, 151, and 152 bar with the 65 mm × 400 mm, 115 mm × 400 mm, 140 mm × 400 mm, and 130 mm × 560 mm connecting tubes, respectively.

We measured the apparent efficiency of the four monolithic columns for the nine analytes (acetanilidine, benzophenone, acetophenone, propiophenone, butyrophenone, valerophenone, hexanophenone, heptanophenone, and octanophenone) contained in the RPLC checkout test sample from Agilent. Fig. 5A–D shows the variation of this efficiency as a function of the retention factors measured, using as hold-up time the retention time of the first eluted compound ($k = 0$). All the results show an obvious impact of the nature of the connecting tubes selected for $k < 3$. As expected, the 0.8 μL detection UV cell generates systematically higher plate counts than the 2.4 μL cell. The highest plate counts were measured with either the Viper tubings or the 65 μm I.D. connectors, which was surprising because the volume of the Viper tubes is five times larger than that of the 65 μm × 400 mm tubings. This is explained by the exceptionally high quality of the design and manufacturing of the connector-column contacts provided by the Viper system, which has an almost zero volume. In contrast, the polymer connectors do not fit well enough to the column inlet (manual cut) and become progressively damaged as they are repeatedly screwed/unscrewed to the columns. The poor performance observed with the other capillary tubes is explained by the presence of a significant free volume between the stainless steel tube and the column endfitting. Since the 130 μm Viper tubings generate a 45% lesser pressure drop than the 65 μm polymer tube and provide similar extra-column band broadening, the Viper connector was selected for the measurement of the corrected column HETP.

4.3. Performance of the monolithic columns

Fig. 6A–D shows the plots versus the mobile phase flow rate of the HETPs corrected for extra-column band broadening of the four new monolithic columns studied. Remarkably, the minimum HETP observed for the non-retained compound (uracil) is between 4 and 5 μm, contrasting with the minimum HETP measured for monolithic columns of the first generation, about 18 μm [17]. This considerable improvement may be related to the narrower inner diameters of these columns (2.3 and 3.2 mm instead of 4.6 mm for the older ones). The HETPs for naphthalene are approximately 10% larger. The performance of the two 3.2 mm I.D. columns is somewhat better than that of the 2.3 mm I.D. columns.

With conventional columns packed with either fully porous or superficially porous particles, the efficiencies of retained compounds at high velocities is systematically higher, with minimum HETP typically around 3.5 μm [72,31], than for non-retained ones. As explained earlier in details [73,35,36], this feature is explained

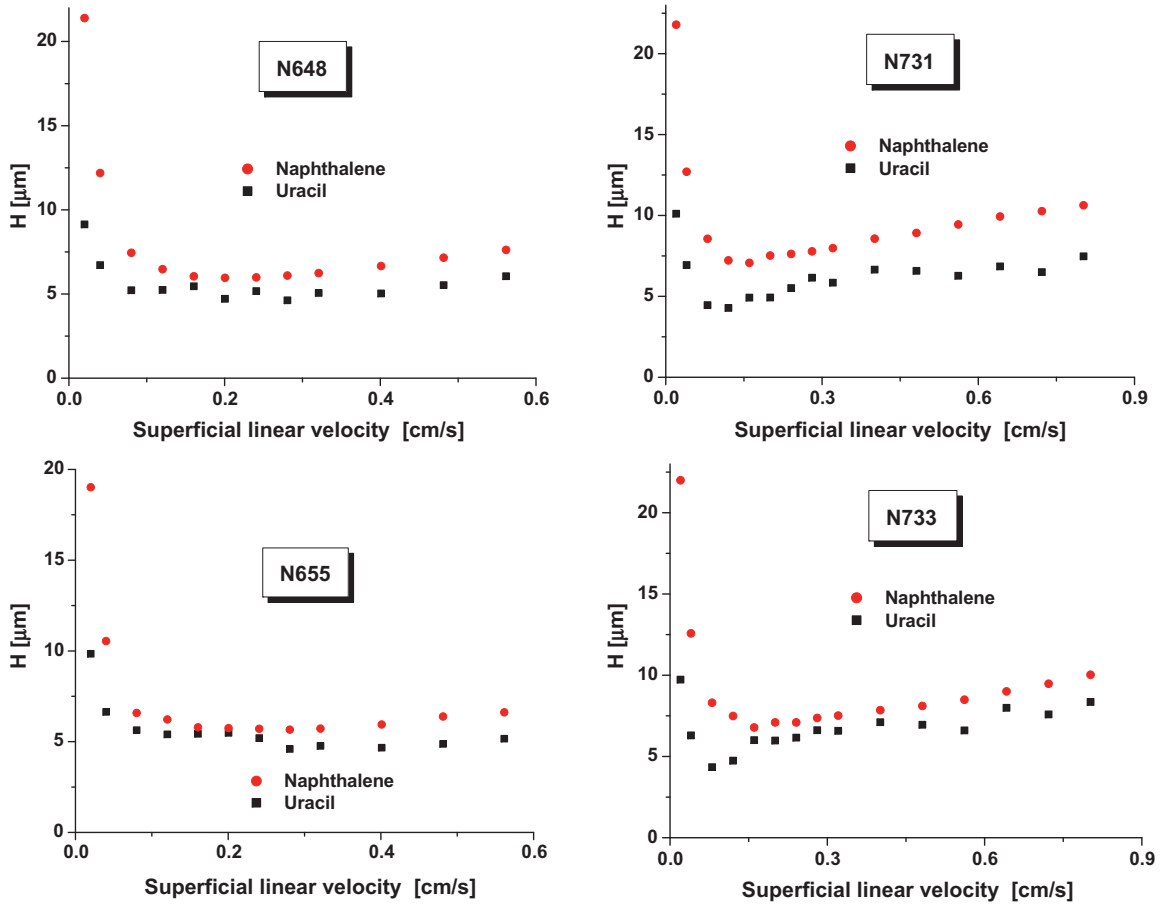

Fig. 6. Corrected HETPs of the four monolithic columns measured for uracil and naphthalene. Note that the minimum HETP (4–5 μm) is larger for the retained than for the non-retained analyte.

by the significant radial trans-column velocity bias that exists in packed columns and was shown by direct measurements at the column outlet using local electrochemical detection [16]. Consequently, because retained compounds spend a longer residence time in the column and diffuse faster through the silica-C_{18} packing particles due to surface diffusion [54], they experience very efficient relaxation of the radial concentration gradient generated by the trans-column velocity bias. Thus the results observed with the new monolithic columns suggest that the eddy diffusion of retained and non-retained compounds proceed at similar velocities. Therefore, the small residual difference between the HETPs of retained and non-retained compounds is mostly explained by the difference in the longitudinal diffusion term, which is larger for retained than for non-retained analytes, due to the significant contribution of surface diffusion to the effective diffusion coefficient of naphthalene along the column.

In the next sections, we report on the values of the eddy diffusion terms derived for uracil and naphthalene in the four monolithic columns, according to Eq. (18), which required the measurements of the longitudinal diffusion term (known from Eq. (2) and the peak parking data given in Fig. 2) and of the solid–liquid mass transfer resistance term. This last term depends on the analyte diffusivity through the porous skeleton (see Eq. (4)). This diffusivity is estimated from the peak parking data and a model of effective diffusion (D_{eff}) in monolithic columns. For this purpose, we need to select the best model of effective diffusion in monolithic columns among the time-averaged (Eq. (7)), the Landauer (Eqs. (9) and (10)), the Garnett (Eq. (11)), and the Torquato (Eqs. (12) and (13)) models of effective diffusion.

4.3.1. Models of effective diffusion in monolithic columns

We follow the same procedure as the one previously used to select the most realistic model of effective diffusion in columns packed with core–shell particles [74]. On the one hand, the intraparticle diffusivity of a non-retained compound through the porous skeleton is first calculated ($\Omega = \epsilon_p \gamma_p F(\lambda_m)$) by combining the measurements of the skeleton porosity and the average pore size (ISEC) with the estimates of the internal obstruction factor (obtained from the Pismen correlation, Eq. (15)) and of the hindrance diffusion factor (obtained from the Renkin correlation, Eq. (16)). The values calculated for Ω are accurate within 40% (due to the 30 and 10% relative errors made on γ_p and $F(\lambda_m)$, respectively) [74]. This accuracy is considered as acceptable. These values of the ratios Ω of the intra-particle diffusivity, $D_{skel.}$, to the bulk diffusion coefficient, D_m, are listed in Table 1 (seventh column). Remarkably, the Ω value for the column N648 (about 0.10) is significantly smaller than those for the other three columns (0.35–0.40), which results from the smaller average pore size of its monolith (65 Å instead of 150–200 Å for the other columns), a result that could have been expected. On the other hand, these same ratios Ω are derived for the non-retained compound uracil from the combination of the results of the peak parking method (experimental D_{eff} values listed in the sixth column of Table 2 for the four monolithic columns tested) and the assumption of a mathematical function f that expresses an effective diffusion model in a monolithic column ($D_{eff} = f(\Omega)$).

Fig. 7 compares the accurate values of Ω (±40%) obtained from the correlations of Pismen and Renkin (x-axis) with the experimental ones (y-axis) derived when assuming the four different models of effective diffusion in monolithic columns that are proposed in

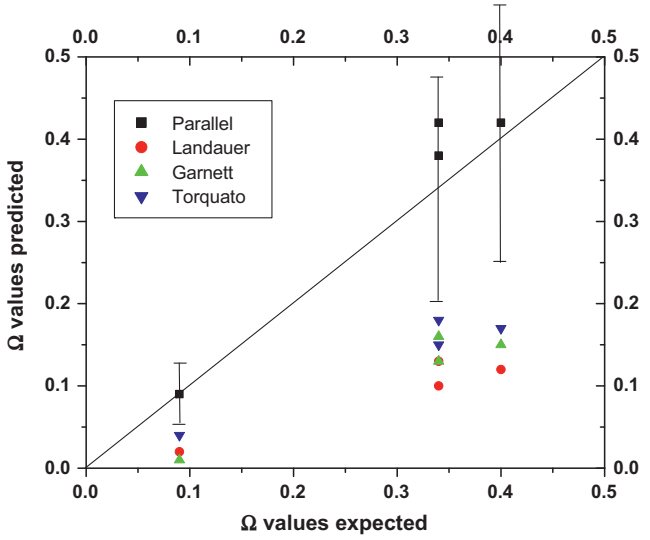

Fig. 7. Comparison between the Ω values calculated from the correlations of Pismen and Renkin (values expected, accuracy within 40%) and those determined by combining the peak parking results (see D_{eff} values in Table 2) and the equations of the four models available for the effective diffusion in monolithic columns (values predicted). Data for the four monolithic columns were used (four data points for each model). The compound is non-retained (uracil). Only the time-averaged parallel diffusion model (all full black squares within the error bar intervals) gives satisfactory results while the Landauer, Garnett, and Torquato models of effective diffusion fail.

Section 2 (y-axis). For a mathematical model f to be physically acceptable, the set of its four data points (one for each column) should be located within the error bars shown in Fig. 7, which are centered on the solid diagonal. Strikingly, only one model seems to be satisfactory, providing acceptable predictions of the intra-skeleton diffusivity of uracil, the simple time-averaged parallel diffusion model.

It should be noted that the other three models underestimate the analyte diffusivity through the porous skeleton by more than 100%. The Torquato model comes as second effective diffusion model but, as the Garnett and the Landauer models, it must be rejected because the error made on the calculated parameter Ω is less than 40%.

4.3.2. Eddy diffusion

The eddy diffusion term was measured according to Eq. (18). For reasons explained in the previous section, the time-averaged model of effective diffusion was used to estimate the values of the skeleton-liquid mass transfer resistance term of the HETP equation, $C_{skel.}u_S$. The values of $C_{skel.}$ are listed in Table 2 (uracil) and Table 3 (naphthalene). The longitudinal diffusion term was measured from the peak parking experiments (see Eq. (2)). The corresponding diffusion coefficient, D_{eff}, and the B term are also listed in these tables. After subtraction of both these HETP terms from the total HETP shown in Fig. 6A–D, the eddy diffusion of columns N731, N733, N648, and N655 are obtained and shown in Fig. 8A–D.

Surprisingly, the eddy diffusion of the non retained uracil is not significantly different from that of the retained naphthalene. This result was observed only once with columns packed with either fully porous or superficially porous particles, one

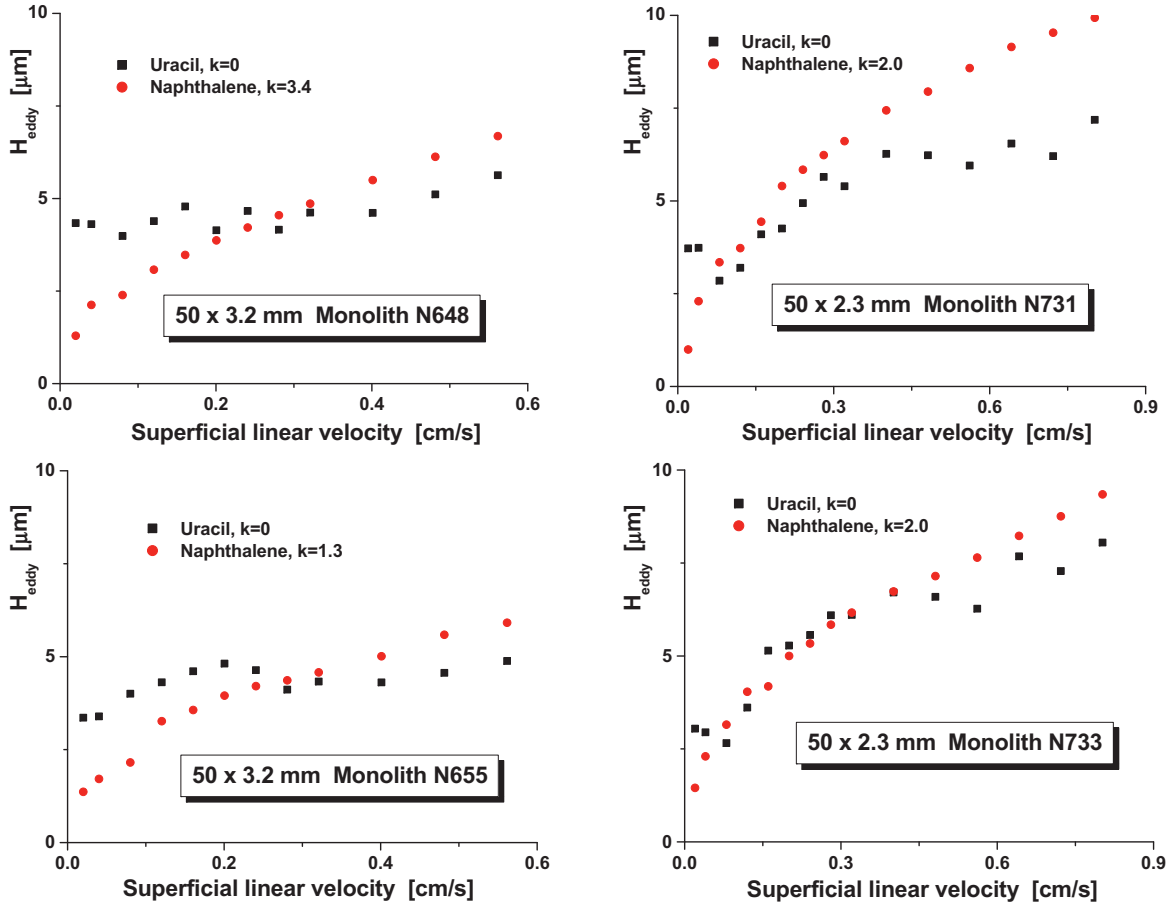

Fig. 8. Eddy diffusion of the four monolithic columns measured for uracil and naphthalene. Note the very similar eddy diffusion obtained for both the retained and non-retained compounds.

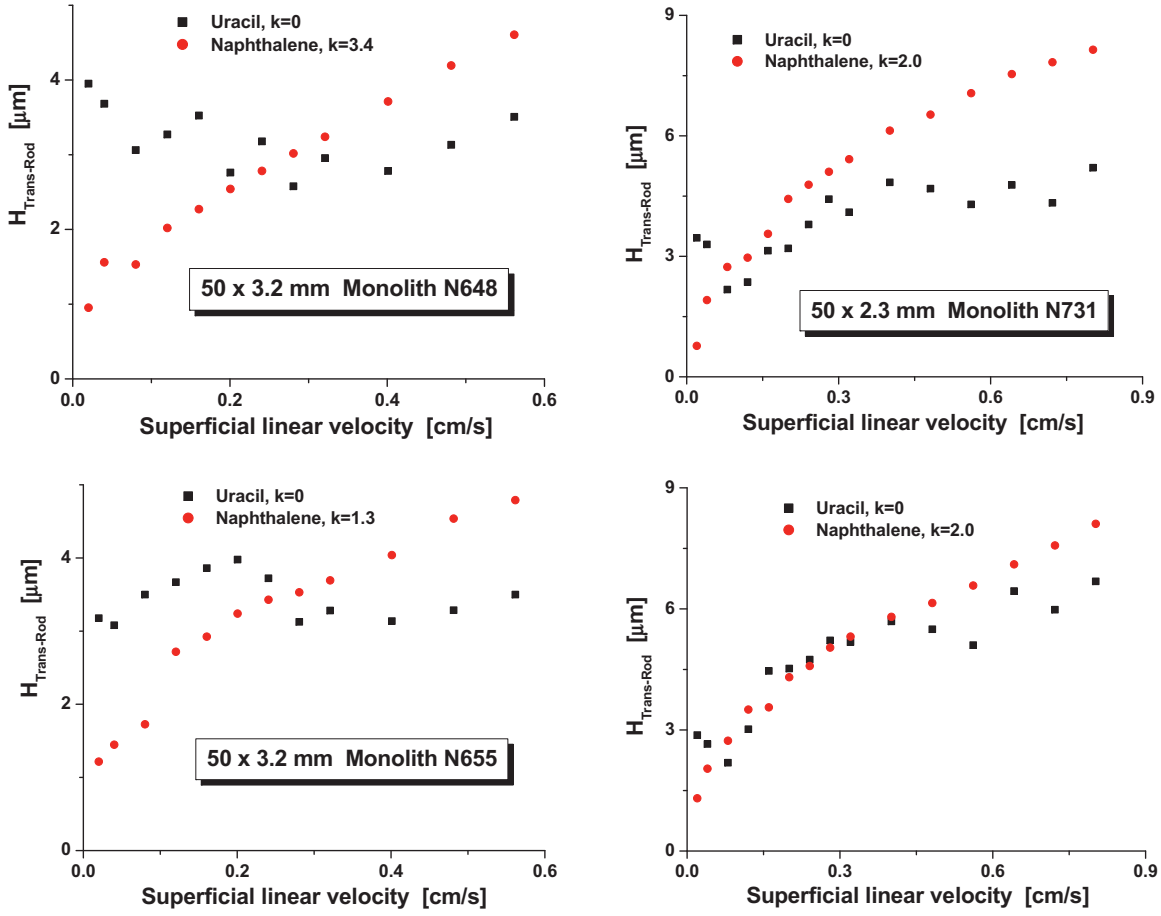

Fig. 9. Trans-rod eddy diffusion of the four monolithic columns measured for uracil and naphthalene.

exceptional column packed with 2.6 μm Kinetex particles that had a minimum reduced plate height of 1.1 [35] (H_{min} = 2.9 μm). This exceptional performance was due to the random nature of the packing process. On the average, the minimum reduced plate heights of core–shell particles were found to be between 1.4 and 1.5 for 2.6 μm Kinetex and 2.7 μm Halo-ES-Peptide [75,76]. Usually, for the first generation of monolithic columns [17] or for all types of packed columns [37,38], the eddy diffusion term of retained compounds is significantly smaller than that of a non-retained compound. As explained earlier, trans-column velocity biases generate radial concentration gradients, which are the major cause of eddy diffusion. Because retained compounds spend a longer time in the column and diffuse faster through it due to fast surface diffusion in RPLC, these gradients relax more efficiently than for a non-retained compound. However, this effect is not obvious with the new monolithic columns given to us by Kyoto Monotech. The advantage of a faster radial diffusivity of analytes becomes useless when the column structure is radially homogeneous. This confirms the radial uniformity of the micro-structure of these new monolithic rods. This might in part be related to the inner diameter of these new monolithic columns being narrower than that of the columns of the first generation of monolithic columns (4.6 mm). Therefore, it appears that a new procedure of synthesis allows the production of radially homogeneous silica monoliths with inner diameters of at least 3.2 mm.

In order to estimate the residual radial heterogeneity of the four monoliths, we estimated their trans-column eddy diffusion term, $H_{Trans\text{-}rod}$. For this purpose, we need estimates of the trans-throughpore and short-range inter-throughpore eddy diffusion terms ($H_{Throughpore}$ and H_{Short}), which will be subtracted from the total eddy diffusion terms. These terms were derived from the calculated values of dispersion in the homogeneous center region of physically reconstructed capillary silica monoliths. They are given by Eqs. (20) and (21). Fig. 9A–D shows the residual trans-rod eddy diffusion terms. The comparison between these figures and Fig. 8A–D shows that the contributions of the trans-throughpore and short-range inter-throughpore eddy diffusion terms to the overall eddy diffusion term are small. In the first generation columns, the residual trans-rod eddy diffusion terms of uracil and

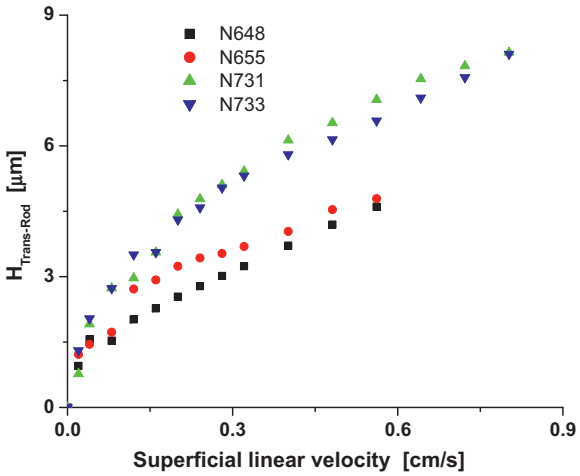

Fig. 10. Comparison between the trans-rod eddy diffusion terms of naphthalene measured for the four new monolithic columns.

toluene were about 20 μm at a superficial linear velocity of 0.4 cm/s [17]. In these new monolithic columns, this term is only 3.2, 3.5, 5.4, and 5.7 μm, respectively, a considerable reduction of the band dispersion due to radial heterogeneity. It is noteworthy that $H_{Trans\text{-}rod}$ contains the contribution of the inlet and outlet distributors to band broadening.

These results are in part due to an improved column structure. The former 4.6 mm I.D. monolithic columns were cladded in a PEEK tube. In the new columns, there are two layers of polymers between the rod and the stainless tube. The flow distributors in the original monolithic columns were made of a polymer disk with six equidistant apertures located about half the column inner radius apart. The ends of the new columns are covered with monolithic silica frits (1 mm thick), possibly allowing a more uniform flow distribution of the eluent at both the column inlet and outlet than disk of the Chromolith columns.

Finally, Fig. 10 compares the trans-rod eddy diffusion terms for naphthalene in the four new monolithic columns. Remarkably, the best performances are observed with the 3.2 mm I.D. columns, which also have the lowest permeabilities and the smallest external porosities. They are those providing the minimum band dispersion. If we assume the length of persistence-of-velocity is of the same order of magnitude as the column length (see detailed analysis and model of trans-column eddy diffusion in [17]), the relative amplitude of the radial velocity gradient across the 3.2 mm I.D. column can be estimated at 1.4%, a value comparable to those observed with 4.6 mm I.D. columns packed with core–shell particles [33]. In contrast, this length was previously estimated at about 3% for the first generation of monolithic columns.

5. Conclusion

In this work, we reported on the mass transfer mechanism of small analytes in 2.3 mm × 50 mm and 3.2 mm × 50 mm new silica monolithic columns prepared by Kyoto Monotech. The average throughpore and skeleton sizes of these prototype columns are about 40% less than those of the monolithic columns of the first generation (Chromolith, Merck). Therefore, the domain size of the new silica monoliths is decreased from 3.3 μm (Chromolith) to 1.9 μm. The average permeability of these new prototype columns is now equivalent to that of columns packed with 4 μm spherical particles, instead of 9 μm for Chromolith columns. Their efficiency is equivalent to those of columns packed with 2–2.5 μm fully porous particles, rather than 9 μm for Chromolith.

This large improvement in column efficiency (+300%) of these new monoliths is primarily explained by their more radially homogeneous structure. To a lesser extent, it is due to a decrease of their domain size. Their residual relative velocity biases are close to 1.5%, a value comparable to those observed for 4.6 mm I.D. columns packed with sub-3 μm core–shell particles, columns that are well known for their exceptionally high efficiency due to a small trans-column eddy diffusion term. Based on the results obtained for the four monolithic columns studied in this work, the best performance was that of the less permeable column (1.35×10^{-14} m^2) that has the smallest average mesopore size (65 Å) and the largest ratio of the skeleton-to-throughpore sizes. Since this column has also the largest domain size (2.3 μm), it seems that the most critical structural parameter is the phase ratio of monolithic columns, the ratio of the stationary phase to the mobile phase volumes, which should be large. Most likely, increasing this phase ratio contributes to increase the distance over which the silica structure remains uniform (up to 3.2 mm). Obviously, the cost of this improvement is a loss in column permeability.

This first step toward the preparation of a second generation of silica based monolithic columns is most encouraging. Although the external structure of the column collapses (albeit reversibly so) for pressures larger than 200 bar, these new columns still provide permeabilities twice and six times larger than those of columns packed with sub-3 μm superficially porous and sub-2 μm fully porous particles, respectively. Therefore, these new columns can provide analyses as efficient but not faster than conventional columns packed with sub-3 μm superficially porous and sub-2 μm fully porous particles operated with conventional or advanced modern HPLC instruments, respectively. Yet, they can potentially compete with the advanced columns over which they have the advantage of operating at lower back pressures, avoiding the nefarious impact of frictional heating on column efficiency.

In a forthcoming paper, we will report on the performance of these new monolithic columns under ultra-fast gradient elution (hold-up time of the order of 5 s). We will compare their performance to those obtained at the same mobile phase velocity with commercially available columns (of the same length) packed with 1.7 μm BEH-C_{18} fully porous and 2.6 μm Kinetex-C_{18} superficially porous particles. The analyses of various authentic and natural complex samples will be discussed.

List of symbols

Roman letters

B	longitudinal diffusion coefficient (m^2/s)
$C_{skel.}$	trans-skeleton mass transfer coefficient (s)
$d_{throughpore}$	average throughpore size (m)
$d_{skel.}$	average monolithic skeleton size (m)
$D_{skel.}$	effective skeleton diffusivity (m^2/s)
D_m	bulk molecular diffusion coefficient (m^2/s)
F_v	flow rate (m^3/s)
H	total column HETP (m)
$H_{Throughpore}$	trans-throughpore eddy diffusion HETP term (m)
H_{Eddy}	Eddy diffusion HETP term (m)
$H_{Long.}$	longitudinal diffusion HETP term (m)
H_{Short}	short-range inter-throughpore eddy diffusion HETP term (m)
$H_{Skel.}$	trans-skeleton mass transfer resistance HETP term (m)
$H_{Trans\text{-}rod}$	trans-rod eddy diffusion HETP term (m)
k	retention factor
k_1	zone retention factor
k_0	specific permeability (m^2)
K_G	Ergun permeability constant
L	monolithic column length (m)
ΔP	pressure drop along the column (Pa)
R_c	column inner radius (m)
T	temperature during the HETP experiments (K)
T_{PP}	temperature during the PP experiments (K)
t_R	elution time (s)
Δt_p	parking residence time (s)
u_S	superficial linear velocity (m/s)
$u_{R,PP}$	migration linear velocity during the peak parking experiments (m/s)

Greek letters

ϵ_e	external column porosity
ϵ_t	total column porosity
ϵ_p	skeleton porosity
γ_e	external obstruction factor
η	eluent viscosity (Pa s)
μ_1	experimental first moment in presence of column (s)
$\mu_{1,ex}$	first moment of the extra-column band profiles (column replaced with a zero volume union connector) (s)
μ'_2	experimental second central moment in presence of column (s^2)

$\mu'_{2,ex}$ second central moment of the extra-column band profiles (column replaced with a zero volume union connector) (s^2)
$\Delta\sigma^2_{PP}$ increment of the peak variance in the parking method experiments (s^2)
ξ_2 parameter in Eq. (8)

Acknowledgements

This work was supported in part by the cooperative agreement between the University of Tennessee and the Oak Ridge National Laboratory. We thank Nobuo Tanaka (GL Sciences, Inc., Kyoto, Japan) for the generous gift of the new prototypes of monolithic columns.

References

[1] K. Nakanishi, N. Soga, J. Am. Ceram. Soc. 74 (1991) 2518.
[2] H. Minakuchi, K. Nakanishi, N. Soga, N. Ishizuka, N. Tanaka, Anal. Chem. 68 (1996) 3498.
[3] H. Minakuchi, K. Nakanishi, N. Soga, N. Ishizuka, N. Tanaka, J. Chromatogr. A 797 (1998) 121.
[4] K. Cabrera, G. Wieland, D. Lubda, K. Nakanishi, N. Soga, H. Minakuchi, K. Unger, Trends Anal. Chem. 17 (1998) 133.
[5] S. Hjerten, J.-L. Liao, J. Chromatogr. 457 (1988) 165.
[6] F. Svec, J. Frechet, Anal. Chem. 64 (1992) 820.
[7] Q. Wang, F. Svec, J. Frechet, J. Chromatogr. A 669 (1994) 230.
[8] M. Kele, G. Guiochon, J. Chromatogr. A 960 (2002) 19.
[9] K. Miyabe, G. Guiochon, J. Phys. Chem. B 106 (2002) 8898.
[10] F. Gritti, W. Piatkowski, G. Guiochon, J. Chromatogr. A 983 (2003) 51.
[11] F. Gritti, W. Piatkowski, G. Guiochon, J. Chromatogr. A 978 (2002) 81.
[12] K. Cabrera, J. Sep. Sci. 27 (2004) 843.
[13] G. Guiochon, J. Chromatogr. A 1168 (2007) 101.
[14] K. Cabrera, 31st International Symposium on High Performance Liquid Phase Separations and Related Techniques (HPLC-2007), Ghent, Belgium, 2007.
[15] K.S. Mriziq, J.A. Abia, Y. Lee, G. Guiochon, J. Chromatogr. A 1193 (2008) 97.
[16] J. Abia, K. Mriziq, G. Guiochon, J. Chromatogr. A 1216 (2009) 3185.
[17] F. Gritti, G. Guiochon, J. Chromatogr. A 1218 (2011) 5216.
[18] D. Hlushkou, S. Bruns, A. Holtzel, U. Tallarek, Anal. Chem. 82 (2010) 7150.
[19] D. Hlushkou, S. Bruns, U. Tallarek, J. Chromatogr. A 1217 (2010) 3674.
[20] S. Bruns, T. Hara, B. Smarsly, U. Tallarek, J. Chromatogr. A 1218 (2011) 5187.
[21] D. Hlushkou, S. Bruns, A. Seidel-Morgenstern, U. Tallarek, J. Sep. Sci. 34 (2011) 2026.
[22] O. Nunez, K. Nakanishi, N. Tanaka, J. Chromatogr. A 1191 (2008) 231.
[23] T. Hara, S. Makino, Y. Watanabe, T. Ikegami, K. Cabrera, B. Smarsly, N. Tanaka, J. Chromatogr. A 1217 (2010) 89.
[24] S. Miyazaki, M. Takahashi, M. Ohira, H. Terashima, K. Morisato, K. Nakanishi, T. Ikegami, K. Miyabe, N. Tanaka, J. Chromatogr. A 1218 (2011) 1988.
[25] M. Rogeberg, S. Wilson, H. Malerod, E. Lundanes, N. Tanaka, T. Greibrokk, J. Chromatogr. A 1218 (2011) 7281.
[26] T. Ikegami, T. Hara, H. Kimura, H. Kobayashi, K. Hosoya, K. Cabrera, N. Tanaka, J. Chromatogr. A 1106 (2006) 112.
[27] R. Hahn, A. Tscheliessnig, P. Bauerhansl, A. Jungbauer, J. Biochem. Biophys. Methods 70 (2007) 87.
[28] F. Gritti, G. Guiochon, J. Chromatogr. A (2011), doi:10.1016/j.chroma.2011.07.014.
[29] U.D. Neue, N. Brady, S. Serpa, P.C. Iraneta, B.A. Alden, T.H. Walter, K. Wyndham, 32nd International Symposium on High Performance Liquid Phase Separations and Related Techniques, Baltimore, MD, May 10–16, 2008.
[30] J.J. DeStefano, T.J. Langlois, J.J. Kirkland, J. Chromatogr. Sci. 46 (2007) 254.
[31] F. Gritti, I. Leonardis, D. Shock, P. Stevenson, A. Shalliker, G. Guiochon, J. Chromatogr. A 1217 (2010) 1589.
[32] F. Gritti, G. Guiochon, J. Chromatogr. A 1217 (2010) 1604.
[33] F. Gritti, I. Leonardis, J. Abia, G. Guiochon, J. Chromatogr. A 1217 (2010) 3219.
[34] G. Guiochon, F. Gritti, J. Chromatogr. A 1218 (2011) 1915.
[35] F. Gritti, G. Guiochon, Chem. Eng. Sci. 65 (2010) 6327.
[36] F. Gritti, G. Guiochon, J. Chromatogr. A 1217 (2012) 2.
[37] F. Gritti, G. Guiochon, J. Chromatogr. A 1217 (2010) 907.
[38] F. Gritti, G. Guiochon, J. Chromatogr. A 1217 (2010) 8167.
[39] F. Gritti, J. Omamogho, G. Guiochon, J. Chromatogr. A 1218 (2011) 7078.
[40] F. Gritti, G. Guiochon, J. Chromatogr. A 1218 (2011) 4452.
[41] P. Stevenson, F. Gritti, G. Guiochon, J. Chromatogr. A 1218 (2011) 8255.
[42] F. Gritti, G. Guiochon, J. Chromatogr. A 1169 (2007) 125.
[43] J. Knox, H. Scott, J. Chromatogr. 282 (1983) 297.
[44] F. Gritti, G. Guiochon, Chem. Eng. Sci. 61 (2006) 7636.
[45] K. Miyabe, Y. Matsumoto, G. Guiochon, Anal. Chem. 79 (2007) 1970.
[46] F. Gritti, G. Guiochon, AIChE J. 57 (2011) 333.
[47] F. Gritti, G. Guiochon, J. Chromatogr. A 1218 (2011) 3476.
[48] F. Gritti, G. Guiochon, Chem. Eng. Sci. 66 (2011) 3773.
[49] J. Giddings, Dynamics of Chromatography, Marcel Dekker, New York, NY, 1965.
[50] F. Gritti, G. Guiochon, Chem. Eng. Sci., in press.
[51] F. Gritti, G. Guiochon, J. Chromatogr. A 1217 (2010) 5137.
[52] M. Al-Bokari, D. Cherrak, G. Guiochon, J. Chromatogr. A 975 (2002) 275.
[53] S. Ergun, Chem. Eng. Prog. 48 (1952) 89.
[54] K. Miyabe, G. Guiochon, J. Chromatogr. A 1217 (2010) 1713.
[55] F. Gritti, G. Guiochon, AIChE J. 57 (2011) 346.
[56] S. Torquato, Random Heterogeneous Materials. Microstructure and Macroscopic Properties, Springer, New York, 2002.
[57] R. Landauer, J. Appl. Phys. 23 (1952) 779.
[58] H. Davis, J. Am. Ceram. Soc. 60 (1977) 499.
[59] J.C.M. Garnett, Philos. Trans. R. Soc. London Ser. B 203 (1904) 385.
[60] S. Torquato, J. Appl. Phys. 58 (1985) 3790.
[61] G. Desmet, S. Deridder, J. Chromatogr. A 1218 (2011) 32.
[62] F. Gritti, G. Guiochon, Anal. Chem. 5329 (2006) 78.
[63] F.M.C.A. Mitzithras, J.H. Strange, J. Mol. Liq. 260 (1992) 273.
[64] L. Pismen, Chem. Eng. Sci. 29 (1974) 1227.
[65] E. Renkin, J. Gen. Physiol. 38 (1954) 225.
[66] J.H. Knox, L. McLaren, Anal. Chem. 36 (1964) 1477.
[67] K. Miyabe, N. Ando, G. Guiochon, J. Chromatogr. A 1216 (2009) 4377.
[68] Y. Miyabe, K. Matsumoto, G. Guiochon, Anal. Chem. 65 (2010) 3859.
[69] D. Ludlum, R. Warner, H. Smith, J. Phys. Chem. 66 (1962) 1540.
[70] P. Dunlop, C. Pepela, B. Steel, J. Am. Chem. Soc. 92 (1970) 6743.
[71] J. Li, P. Carr, Anal. Chem. 69 (1997) 2530.
[72] F. Gritti, G. Guiochon, J. Chromatogr. A 1217 (2010) 1485.
[73] F. Gritti, G. Guiochon, AIChE J. 56 (2010) 1495.
[74] F. Gritti, G. Guiochon, Chem. Eng. Sci. 66 (2011) 6168.
[75] F. Gritti, G. Guiochon, J. Chromatogr. A, in preparation.
[76] F. Gritti, G. Guiochon, J. Chromatogr. A, in preparation.